# Symmetry breaking and geometric confinement in $VO_2$: Results from a three-dimensional infrared nano-imaging

Mengkun Liu,[1] Martin Wagner,[1] Jingdi Zhang,[2] Alexander McLeod,[1] Salinporn Kittiwatanakul,[3] Zhe Fei,[1] Elsa Abreu,[2] Michael Goldflam,[1] Aaron J. Sternbach,[1] Siyuan Dai,[1] Kevin G. West,[4] Jiwei Lu,[4] Stuart A. Wolf,[3,4] Richard D. Averitt,[1,2] and D. N. Basov[1,a)]

[1]*Department of Physics, University of California, San Diego, La Jolla, California 92093, USA*
[2]*Department of Physics, Boston University, Boston, Massachusetts 02215, USA*
[3]*Department of Physics, University of Virginia, Charlottesville, Virginia 22904, USA*
[4]*Department of Materials Science and Engineering, University of Virginia, Charlottesville, Virginia 22904, USA*

(Received 31 October 2013; accepted 11 March 2014; published online 25 March 2014)

Epitaxial strain can play an important role in controlling the local phase dynamics of transition metal oxides. With scattering-type scanning near-field optical microscopy, we visualize the three dimensional landscape of phase inhomogeneity in strained $VO_2$ films grown on $[100]_R$ $TiO_2$ substrates. We demonstrate that three different symmetries are spontaneously broken in the vicinity of the $VO_2$ phase transition: (1) Monoclinic-tetragonal (rutile) crystal symmetry breaking due to the structural phase transition, (2) in-plane (x-y plane) rotational symmetry breaking due to the formation of periodic strain domains, and (3) out-of-plane (z-axis) mirror symmetry breaking at the film cross-section due to substrate-induced epitaxial strain. © *2014 AIP Publishing LLC*. [http://dx.doi.org/10.1063/1.4869558]

Symmetry-breaking phase transitions are ubiquitous phenomena in condensed matter physics. In strongly correlated electron materials, broken symmetries can result in mesoscopic separation of multiple phases in the course of a solid-solid phase transition.[1–7] Uniaxial strain, as a controllable parameter, can be exploited as a versatile tool to modify and tame the domain texture associated with the underlying symmetry change induced by lattice distortion.[4] Compared to other phase control mechanisms such as electrostatic gating,[8] ultrafast photoexcitation[9,10] and magnetic field switching,[7] strain has the distinct advantage of leading to a three-dimensional (3D) geometric modification yielding well-defined changes in the local environment. In order to intuitively understand the strain behavior and to clarify its role in compounds displaying a symmetry-breaking metal-insulator transition (MIT), it is imperative to monitor the 3D evolution of the structural and electronic properties of canonical phase change materials under substantial strain. The sample material chosen for this study, vanadium dioxide ($VO_2$), exhibits a phase transition temperature ($T_c$) close to room temperature (340 K) and serves as an ideal candidate.[11]

Recent advances in the fabrication and characterization of high quality $VO_2$ crystals with various substrates and geometrical configurations have finally allowed for microscopic control of this material, helping to unravel the intrinsic physics of its metal-insulator transition[12–15] that has eluded a complete description for decades. For example, tremendous effort has been made in studying free standing/supported $VO_2$ nanobeams and nanoplatelets.[14–25] Under external strain, these geometrically constrained $VO_2$ systems reveal unique patterns of structural and electronic domain formation which are also of interest in the context of potential applications.[17,26] In unstrained polycrystalline $VO_2$ films, the percolation process dominates through the phase transition, and the metallic puddles are randomly distributed.[12] However, in strained epitaxial $VO_2$ films, the phase separation involves formation of unidirectional mesoscopic stripes.[27] In this work, we investigate the evolution of stripe patterns in strained $VO_2$ films (on $[100]_R$ $TiO_2$ substrates) in greater detail. Using IR near-field microscopy, we directly visualize the spontaneous 3D distribution of unidirectional metallic domains and reveal that the formation of the stripe state is governed by the crystal symmetry as well as geometric confinement. Specifically, we visualize two important processes: (i) The percolation and orientation of metallic stripes along the monoclinic c axis and (ii) strain-induced metallic nucleation build-up at the sample-substrate interface. We also demonstrate that the orientational preference of these stripes and the occurrence of complex domain patterns such as domain junctions and bifurcations depend strongly on the lateral geometry of the crystals. In cases of strong lateral confinement, the stripe patterns retrieve the character of $VO_2$ nanobeams.[15,21,28]

One unique way to study 3D dielectric properties of materials, as first demonstrated here, is by using scattering-type scanning near-field optical microscopy (s-SNOM). Based on a hybrid of an atomic force microscope (AFM) and an infrared (IR) laser, s-SNOM enables the study of optical properties of materials at nanometer length scale.[29,30] In our apparatus, IR light pulses are generated through difference-frequency generation (DFG) with a 40 MHz Er fiber oscillator. The pulses are focused onto the AFM tip, and the amplitude of the back-scattered IR electric field is demodulated at different harmonics ($n = 1, 2, 3\ldots$) of the tip's tapping frequency to yield "near-field signals" $S_n$. Higher harmonic signals ($n = 2, 3, 4\ldots$) reflect the genuine near-field interaction between the tip and the sample

a)Author to whom correspondence should be addressed. Electronic mail: dbasov@physics.ucsd.edu

 

surface, and therefore contain information on the local dielectric properties. The s-SNOM approach affords optical resolution down to 10–20 nm (limited only by the AFM tip radius): A virtue routinely employed in IR nano-imaging and spectroscopy.[29–32] We show that this technique is equally well suited for probing cross-sectional properties of thin film samples.

In Fig. 1, we schematically show "planar" and "cross-sectional" nano-imaging modalities. Fig. 1(a) presents the "planar" procedure: A commonplace scheme for s-SNOM measurements. We note that instead of a temperature controlled sample stage, here we can introduce an additional near-IR pump beam with a wavelength of 1.56 $\mu$m to *thermally* excite the film.[33] In order to investigate the sample cross-section at elevated temperatures, the thin film sample can also be cleaved and mounted *"vertically"* on a temperature controlled stage (Fig. 1(b)). Cross-sectional raster scans yield AFM and near-field signals that reveal the evolution of the film properties from the substrate/sample interface to the sample surface. Note that the sample is intentionally tilted by a small angle so that one can simultaneously study the substrate, the film cross-section, and the adjacent sample surface.

The 250 nm $VO_2$ films studied in this work were deposited on a $[100]_R$ $TiO_2$ substrate.[34] Room temperature X-ray diffraction (XRD) experiments confirm their single-crystal nature and identify the lattice parameters of these samples. The XRD results (not shown) are indicative of a compressive strain along $b_R$ ($[010]_R$) and a tensile strain along $c_R$ ($[001]_R$), in agreement with previous studies.[35,36] The relatively large film thickness (250 nm) leads to strain release, therefore causing the formation of cracks that occur along the rutile $c_R$ axis ($[001]_R$), as identified by both AFM and scanning electron microscopy (SEM).[36] The micro-beams formed between the cracks have widths ($W$) ranging from ~0.5 to 5 $\mu$m (cracks that define beam widths are marked by white dashed lines in Figs. 2 and 3).

In Fig. 2, we present the main findings of this work: Pump induced spontaneous symmetry breaking in a 250 nm

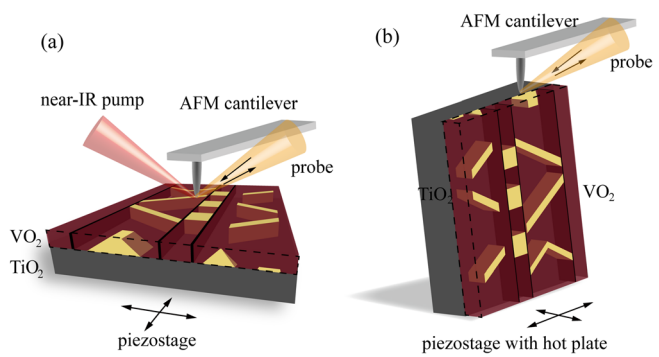


FIG. 1. Schematic of the two imaging modalities for 3D s-SNOM measurements. (a) Experimental geometry for planar near-field measurements: The sample surface is thermally excited by a near-IR pump (1.56 $\mu$m wavelength), yielding an equivalent local temperature tunable between 295 K to ~360 K. (b) Experimental geometries for cross-sectional near-field imaging. The sample can be cleaved to less than 1 mm in height and mounted vertically on a hot plate which adjusts the sample temperature between 295 K and 400 K. We have chosen not to employ near-IR pump excitation at cross-sectional scans in order to avoid local thermal gradient at the sample-substrate interface.

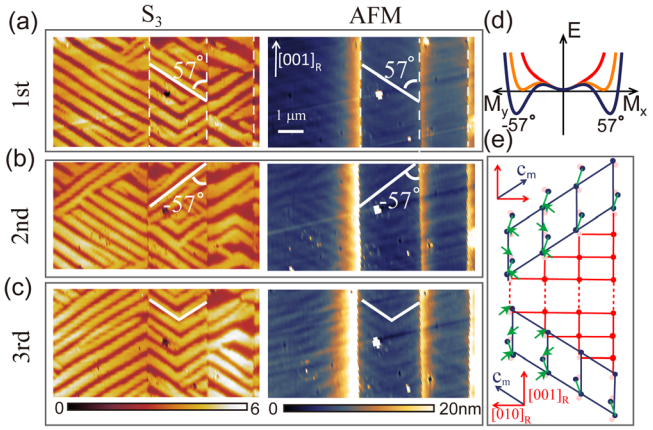


FIG. 2. Pump sequence dependent near-field and AFM images. (a) Simultaneously acquired near-field $S_3$ and AFM images with 18.8 mW pump excitation. Between ((a) and (b)), ((b) and (c)), the pump was blocked and unblocked in less than 1 s. Following each re-illumination, new patterns are formed which display a spontaneous structural symmetry breaking, with stripes aligning along two possible orientations of the monoclinic c axis (indicated by the white lines in (a)–(c)). (d) Schematic energy landscape of $VO_2$. $M_x$ and $M_y$ define two monoclinic lattice modes with mirror symmetry (the axis of symmetry is the rutile c axis): Red: rutile favored state, Blue: monoclinic favored state; Orange: coexistence of the two phases. (e) Crystal structure of $VO_2$ in $[100]_R$ plane: Red: rutile lattice; Blue: monoclinic (M1) lattice; Green lines: V–V dimer pairs. Green arrows: The direction of the movement of V atoms.

$[100]_R$ $VO_2$ film. Figs. 2(a)–2(c) show pump-sequence dependent near-field $S_3$ and AFM images acquired at the same location of the $VO_2$ surface. The 18.8 mW near-IR pump, which locally elevates the sample temperature to ~334 K (temperature assignment described in SI), induces a highly oriented stripe state as revealed by the near-field $S_3$ images and the AFM topography. In these images, the metallic stripes show a herringbone pattern with two distinct

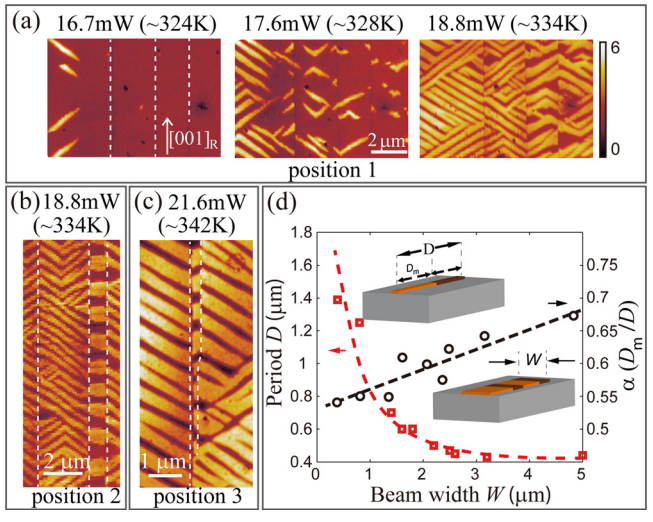


FIG. 3. Near-field study of the $VO_2$ film surface at different pump intensities. (a) Near field images ($S_3$) acquired at 16.7 mW, 17.6 mW, and 18.8 mW pump powers at sample position 1. The $c_R$ axis and crack positions are indicated by the white arrow and dashed lines, respectively. ((b) and (c)) near-field images ($S_3$) acquired at 18.8 mW and 21.6 mW pump power at positions 2 and 3, respectively. (d) Beam width (W) dependent pattern periodicity D (defined in the inset schematic) extracted from near-field images acquired at 18.8 mW pump power (red squares). The volume ratio of metallic phase ($D_m$/D) is also estimated based on multiple near-field images (black circles). Dashed lines are provided as a guide for the eye.

orientations, forming ~57° angles with mirror symmetry. This finding is consistent with the two equivalent in-plane orientations of the *monoclinic* c axis.[37,38] However, it differs from both our previous study[27] or from the cases of $VO_2$ nanobeams[15,17–19,21] in which the orientation of the stripes was aligned along the crystal axis of the *rutile* phase. Quickly blocking the pump beam for less than 1 s and then re-illuminating the region of interest under the identical conditions erases the initial pattern and produces a new, reconstructed pattern in both $S_3$ and AFM images. The newly formed patterns conform to the same possible directions (+57° or −57°) but otherwise bear no resemblance to the initial patterns. Therefore, the images in Fig. 2 are indicative of a spontaneous symmetry breaking phase separation.[4,39,40] These results are further confirmed by the spontaneous lattice domain reformation in the AFM images, always acquired simultaneously with the near-field measurements.

We propose that a Landau-like free elastic energy analysis can qualitatively depict our observations of the formation of the two symmetric stripe states in $VO_2$. This same argument was originally introduced for perovskite manganite systems.[4] As the material goes through a transition from a parent phase to a distorted phase of lower symmetry, long-range elastic modes couple to the allowed short range modes ($M_x$ and $M_y$), yielding two energy minima with equal potentials and mirror symmetry. In our case, the two energy minima correspond to two different monoclinic *c*-axis orientations with mirror symmetry at ~57° with respect to the rutile c axis (see Fig. 2(d) and also online supplementary materials[33]). An immediate implication of this scenario is the existence of two spontaneously oriented vanadium–vanadium (V–V) dimer pairs with mirror symmetry in the monoclinic state. In order to clarify the nature of the three coexistent states in our $VO_2$ samples (57° and −57° monoclinic together with the rutile state), in Fig. 2(e), we display one possible lattice geometry which breaks symmetry in the $[100]_R$ plane. The green arrows indicate the movement of vanadium atoms, and the green lines are V–V dimer pairs. Symmetry breaking during the formation of V–V dimer pairs together with monoclinic (blue)-rutile (red) phase coexistence can lead to the long-range herringbone pattern we observe in our near-field imaging.

Fig. 2 clearly demonstrates that the observed phase separation does not arise from a permanent "built-in" strain field but rather is a spontaneous cooperative process. This process also closely resembles a Martensitic transformation under uniaxial strain.[41–46] In the following, we present a detailed 3D near-field imaging study at the surface and the cross-section of the film, in order to grasp a deeper understanding of the strain induced geometric phase separation and symmetry breaking.

In Fig. 3, we present pump power dependent near-field images taken at three different locations across the $VO_2$ film surface. We have observed several interesting features due to the presence of the cracks and the variation of the beam width (*W*) along c axis: (1) At relatively low pump power, the metallic stripes emerge mainly at the center of the micro-beams (Figs. 3(a) and 3(b)); (2) the average periodicity of the stripes (*D*) and their orientation varies systematically with the width of the beams (*W*) (Figs. 3(b) and 3(c)). In the narrowest beams ($W < 1\,\mu m$), the stripes align nearly perpendicular to the $c_R$ axis (see Figs. 3(b) and 3(c)), consistent with earlier reports on $VO_2$ nanobeams.[15,19,21] (3) The domain bifurcations/junctions, where stripes with identical/distinct orientations intersect, can only be observed in micro-beams with large widths ($W > 1\,\mu m$) (see also Fig. 2). In beams with small widths ($W < 1\,\mu m$), the system is geometrically confined and, therefore, free of complex domain structures.

The systematic relationship between *W*, *D*, and $\alpha$ revealed by our images is plotted in Fig. 3(e). Here, $\alpha$ is the averaged volume fraction of the metallic phase, defined by $\alpha = \frac{D_m}{D}$, where $D_m$ is the averaged width of the metallic stripes. It is clear that with decreasing *W*, the domain-wall energy gradually suppresses the elastic misfit energy due to epitaxial strain release, leading to a reorientation of the stripes and increasing *D* to minimize the domain-wall energy. For the beams with smallest widths, this trend reduces to the behavior reported in nanobeams.[47]

Fig. 4 shows cross-sectional s-SNOM images of the film acquired using the procedure described in Fig. 1(b). To elucidate the importance of strain, we focus our discussion on representative data collected at 335 K, five degrees below the bulk transition temperature ($T_c = 340$ K). Three adjacent regions are shown with characteristic near-field ($S_3$) cross section patterns: A line (upper right), a triangle (middle), and a trapezoid (lower left). Since a larger value in the near-field signal ($S_3$) corresponds directly to a higher IR conductivity,[29,48] metallic nucleation at the film cross section and its adjacent film surface can be mapped out through these images. From Fig. 4, it is evident that the nucleation pattern varies between different locations. Nevertheless, within all the cross-section regions we studied, metallic nucleation preferentially occurs at the film/substrate interface where the epitaxial strain is the strongest. These metallic regions can extend up to the sample surface, where a stripe like pattern emerges in the plane of the film (e.g., sample surface at the lower left of Fig. 4).

Since the sample temperature was maintained at $T < T_{bulk}$ ($T_{bulk} = 340$ K, defined as the critical insulator to

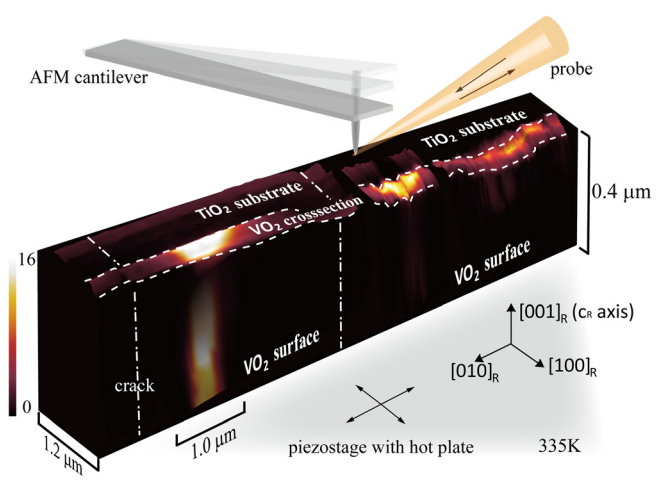


FIG. 4. Near-field IR study of the $VO_2$ film cross-section at a fixed temperature (335 K). The $VO_2$ film thickness is ~250 nm. Three representative images composing the near field signal ($S_3$) reveal epitaxial strain-induced metallic stripe nucleation though the $VO_2$ cross-section and at the adjacent sample surface. Note that the schematic AFM cantilever is not to scale.

metal phase transition temperature at the bulk limit without strain), the patterns defined by the emergent metallic domains in Figs. 2–4 allow us to visualize the local strain induced phase transition. Our observations show that higher epitaxial strain along $c_R$ axis promotes nucleation of local metallic regions at: $T_{local} < T_{bulk}$. We register these effects in the vicinity of the $VO_2/TiO_2$ interface and at the center of $VO_2$ micro-beams. These observations suggest that the local strain at these nucleated regions is highly compressive along $c_R$ axis despite the fact that the global strain is tensile along $c_R$. This alternation of the local tensile-compressive-tensile strain environment leads to the observed variations in nucleation temperature $T_{local}$. Therefore, a macroscopic transition temperature $T_{global}$ is not sufficient to describe the complicated phase transition in a strained thin film.[49,53–56] Use of the nomenclature $T_{local}$ is more appropriate and may serve as key for interpreting the macroscopic properties of strained films.

Our results have demonstrated that performing both cross-sectional and planar near-field mapping enables a nanoscopic investigation of spontaneous symmetry breaking in a 3D geometry. Metallic stripes are stabilized by strain-induced structural phase separation at temperatures below $T_{bulk}$, manifesting in distinct herringbone patterns of insulating and conducting regions. The formation of these patterns strongly depends on the local sample geometry and strain relaxation. Cross-sectional images reveal preferential metallic nucleation at the film/substrate interface where the epitaxial strain is the strongest, whereas planar images reveal spontaneous crystal symmetry breaking during the phase separation. Further developments of s-SNOM techniques will enable characterization of the interface/layered structure in phase separated systems at cryogenic temperatures.[31] Promising candidates of considerable interest for future study include Mott–Hubbard insulators,[50] perovskite manganites,[5] multiferroics[51] and layered superconductors.[52]

M.K.L acknowledges support from Helmholtz Virtual Institute MEMRIOX. D.N.B. acknowledges support from ARO. Development of nano-optics capabilities at UCSD is supported by DOE-BES. R.D.A. acknowledges support from DOE-BES under Grant No. DE-FG02-09ER46643. A.S.M. acknowledges support from the Basic Energy Sciences initiative of the U.S. Dept. of Energy (DOE-BES). E.A. acknowledges support from Fundação para a Ciência e a Tecnologia, Portugal, through a doctoral degree fellowship (No. SFRH/BD/47847/2008). S.K., J.L., and S.A.W. are grateful for the support from the Nanoelectronics Research Initiative (NRI) and VMEC.

[1]H. E. Mohottala, B. O. Wells, J. I. Budnick, W. A. Hines, C. Niedermayer, L. Udby, C. Bernhard, A. R. Moodenbaugh, and F.-C. Chou, Nature Mater. **5**, 377 (2006).
[2]V. B. Shenoy, D. D. Sarma, and C. N. R. Rao, Chemphyschem **7**, 2053 (2006).
[3]E. Dagotto, T. Hotta, and A. Moreo, Phys. Rep. **344**, 1 (2001).
[4]K. Ahn, T. Lookman, and A. Bishop, Nature **428**, 401 (2004).
[5]T. Z. Ward, J. D. Budai, Z. Gai, J. Z. Tischler, L. Yin, and J. Shen, Nat. Phys. **5**, 885 (2009).
[6]Z. Sheng, M. Nakamura, F. Kagawa, M. Kawasaki, and Y. Tokura, Nat. Commun. **3**, 944 (2012).
[7]K. Lai, M. Nakamura, W. Kundhikanjana, M. Kawasaki, Y. Tokura, M. A. Kelly, and Z.-X. Shen, Science **329**, 190 (2010).
[8]J. Jeong, N. Aetukuri, T. Graf, T. D. Schladt, M. G. Samant, and S. S. P. Parkin, Science **339**, 1402 (2013).
[9]A. Cavalleri, C. Toth, C. W. Siders, J. A. Squier, F. Raksi, P. Forget, and J. C. Kieffer, Phys. Rev. Lett. **87**, 237401 (2001).
[10]M. Liu, H. Y. Hwang, H. Tao, A. C. Strikwerda, K. Fan, G. R. Keiser, A. J. Sternbach, K. G. West, S. Kittiwatanakul, J. Lu, S. A. Wolf, F. G. Omenetto, X. Zhang, K. A. Nelson, and R. D. Averitt, Nature **487**, 345 (2012).
[11]F. J. Morin, Phys. Rev. Lett. **3**, 34 (1959).
[12]M. M. Qazilbash, M. Brehm, B.-G. Chae, P. C. Ho, G. O. Andreev, B.-J. Kim, S. J. Yun, A. V. Balatsky, M. B. Maple, F. Keilmann, H.-T. Kim, and D. N. Basov, Science **318**, 1750 (2007).
[13]M. M. Qazilbash, A. Tripathi, A. A. Schafgans, B.-J. Kim, H.-T. Kim, Z. Cai, M. V. Holt, J. M. Maser, F. Keilmann, O. G. Shpyrko, and D. N. Basov, Phys. Rev. B **83**, 165108 (2011).
[14]A. C. Jones, S. Berweger, J. Wei, D. Cobden, and M. B. Raschke, Nano Lett. **10**, 1574 (2010).
[15]J. Wu, Q. Gu, B. S. Guiton, N. P. De Leon, L. Ouyang, and H. Park, Nano Lett. **6**, 2313 (2006).
[16]A. Tselev, E. Strelcov, I. A. Luk'yanchuk, J. D. Budai, J. Z. Tischler, I. N. Ivanov, K. Jones, R. Proksch, S. V. Kalinin, and A. Kolmakov, Nano Lett. **10**, 2003 (2010).
[17]B. Hu, Y. Ding, W. Chen, D. Kulkarni, Y. Shen, V. V. Tsukruk, and Z. L. Wang, Adv. Mater. **22**, 5134 (2010).
[18]W. Fan, S. Huang, J. Cao, E. Ertekin, C. Barrett, D. R. Khanal, J. C. Grossman, and J. Wu, Phys. Rev. B **80**, 241105 (2009).
[19]S. Zhang, J. Y. Chou, and L. J. Lauhon, Nano Lett. **9**, 4527 (2009).
[20]Z. Tao, T.-R. T. Han, S. D. Mahanti, P. M. Duxbury, F. Yuan, C.-Y. Ruan, K. Wang, and J. Wu, Phys. Rev. Lett. **109**, 166406 (2012).
[21]J. Cao, E. Ertekin, V. Srinivasan, W. Fan, S. Huang, H. Zheng, J. W. L. Yim, D. R. Khanal, D. F. Ogletree, J. C. Grossman, and J. Wu, Nat. Nanotechnol. **4**, 732 (2009).
[22]A. Tselev, V. Meunier, E. Strelcov, W. A. Shelton, I. A. Luk'yanchuk, K. Jones, R. Proksch, A. Kolmakov, and S. V. Kalinin, ACS Nano **4**, 4412 (2010).
[23]J. Cao, Y. Gu, W. Fan, L. Q. Chen, D. F. Ogletree, K. Chen, N. Tamura, M. Kunz, C. Barrett, J. Seidel, and J. Wu, Nano Lett. **10**, 2667 (2010).
[24]T. J. Huffman, P. Xu, M. M. Qazilbash, E. J. Walter, H. Krakauer, J. Wei, D. H. Cobden, H. A. Bechtel, M. C. Martin, G. L. Carr, and D. N. Basov, Phys. Rev. B **87**, 115121 (2013).
[25]J. H. Park, J. M. Coy, T. S. Kasirga, C. Huang, Z. Fei, S. Hunter, and D. H. Cobden, Nature **500**, 431 (2013).
[26]R. Xie, C. T. Bui, B. Varghese, Q. Zhang, C. H. Sow, B. Li, and J. T. L. Thong, Adv. Funct. Mater. **21**, 1602 (2011).
[27]M. K. Liu, M. Wagner, E. Abreu, S. Kittiwatanakul, A. McLeod, Z. Fei, M. Goldflam, S. Dai, M. M. Fogler, J. Lu, S. A. Wolf, R. D. Averitt, and D. N. Basov, Phys. Rev. Lett. **111**, 096602 (2013).
[28]B. Hu, Y. Zhang, W. Chen, C. Xu, and Z. L. Wang, Adv. Mater. **23**, 3536 (2011).
[29]S. Amarie, T. Ganz, and F. Keilmann, Opt. Express **17**, 21794 (2009).
[30]J. M. Atkin, S. Berweger, A. C. Jones, and M. B. Raschke, Adv. Phys. **61**, 745 (2012).
[31]H. U. Yang, E. Hebestreit, E. E. Josberger, and M. B. Raschke, Rev. Sci. Instrum. **84**, 023701 (2013).
[32]D. Bonnell, D. Basov, M. Bode, U. Diebold, S. Kalinin, V. Madhavan, L. Novotny, M. Salmeron, U. Schwarz, and P. Weiss, Rev. Mod. Phys. **84**, 1343 (2012).
[33]See supplementary material at http://dx.doi.org/10.1063/1.4869558 for a complete description of the experimental details of thermal photo excitation and analysis of the $VO_2$ crystal symmetry.
[34]K. G. West, J. Lu, J. Yu, D. Kirkwood, W. Chen, Y. Pei, J. Claassen, and S. A. Wolf, J. Vac. Sci. Technol., A **26**, 133 (2008).
[35]S. Kittiwatanakul, J. Lu, and S. A. Wolf, Appl. Phys. Express **4**, 091104 (2011).
[36]E. Abreu, M. Liu, J. Lu, K. G. West, S. Kittiwatanakul, W. Yin, S. A. Wolf, and R. D. Averitt, New J. Phys. **14**, 083026 (2012).
[37]J. B. Goodenough, J. Solid State Chem. **3**, 490 (1971).
[38]S. Lysenko, V. Vikhnin, F. Fernandez, A. Rua, and H. Liu, Phys. Rev. B **75**, 075109 (2007).
[39]R. M. Wentzcovitch, W. W. Schulz, and P. B. Allen, Phys. Rev. Lett. **72**, 3389 (1994).
[40]J. Brews, Phys. Rev. B **1**, 2557 (1970).
[41]G. Barsch, B. Horovitz, and J. Krumhansl, Phys. Rev. Lett. **59**, 1251 (1987).

[42]J. A. Krumhansl, J. Phys. IV France **05**, C2-3-C2-14 (1995).
[43]I. Khakhaev, Phys. Solid State **36**, 898 (1994).
[44]K. Bhattacharya, S. Conti, G. Zanzotto, and J. Zimmer, Nature **428**, 55 (2004).
[45]S. Shenoy, T. Lookman, A. Saxena, and A. Bishop, Phys. Rev. B **60**, R12537 (1999).
[46]K. Bhattacharya and R. D. James, Science **307**, 53 (2005).
[47]Y. Cheng, T. Zhang, Y. Cai, K. M. Ho, K. K. Fung, and N. Wang, Eur. J. Inorg. Chem. **2010**, 4332.
[48]M. M. Qazilbash, M. Brehm, G. O. Andreev, A. Frenzel, P. C. Ho, B.-G. Chae, B.-J. Kim, S. J. Yun, H.-T. Kim, A. V. Balatsky, O. G. Shpyrko, M. B. Maple, F. Keilmann, and D. N. Basov, Phys. Rev. B **79**, 075107 (2009).
[49]Within a single phase Mott picture, one expects $T_{global} > 340\,K$ for $VO_2$ films deposited on $[110]_R$ and $[100]_R$ $TiO_2$ substrates (with an overall tensile strain along $c_R$). One also anticipates $T_{global} < 340\,K$ for films deposited on $[011]_R$ and $[001]_R$ $TiO_2$ substrates due to an overall compressive strain along $c_R$.[8,34,35,53–56] As clearly demonstrated in Figures 2–4, the spontaneous 3D strain redistribution at mesoscopic scales amends the general trend of this semi-empirical "$T_{global}$"-strain relationship previously observed.
[50]M. Dumm, S. Komiya, Y. Ando, and D. Basov, Phys. Rev. Lett. **91**, 077004 (2003).
[51]J. Seidel, L. W. Martin, Q. He, Q. Zhan, Y.-H. Chu, A. Rother, M. E. Hawkridge, P. Maksymovych, P. Yu, M. Gajek, N. Balke, S. V. Kalinin, S. Gemming, F. Wang, G. Catalan, J. F. Scott, N. A. Spaldin, J. Orenstein, and R. Ramesh, Nature Mater. **8**, 229 (2009).
[52]S. A. Kivelson, I. P. Bindloss, V. Oganesyan, J. M. Tranquada, A. Kapitulnik, and C. Howald, Rev. Mod. Phys. **75**, 1201 (2003).
[53]Y. Muraoka and Z. Hiroi, Appl. Phys. Lett. **80**, 583 (2002).
[54]B. Lazarovits, K. Kim, K. Haule, and G. Kotliar, Phys. Rev. B **81**, 115117 (2010).
[55]J. Lu, K. G. West, and S. A. Wolf, Appl. Phys. Lett. **93**, 262107 (2008).
[56]K. Nagashima, T. Yanagida, H. Tanaka, and T. Kawai, Phys. Rev. B **74**, 172106 (2006).